Chalcogenide Letters Vol. 12, No. 9, September 2015, p. 461 - 475

NONISOTHERMAL CRYSTALLIZATION KINETICS OF THE AMORPHOUS $Cu_{18}As_{30}Te_{52}$ ALLOY: MODEL-FREE AND MODEL-FITTING ANALYSIS

A.A. ELABBAR[a], M. ABU EL-OYOUN[a,b], A.A. ABU-SEHLY[b], N. AFIFY[b]
[a]*Department of Physics, Faculty of Science, Taibah University, PO Box 30002, Madina, Saudi Arabia*
[b]*Department of Physics, Faculty of Science, Assuit University, PO Box 71515, Assuit, Egypt*

The kinetics of the crystallization process of glassy $Cu_{18}As_{30}Te_{52}$ alloy was studied under nonisothermal conditions using differential scanning calorimetry (DSC). Three exothermic peaks were observed, indicating the presence of three distinct stages of crystallization. The kinetic parameters (the effective activation energy (*E*), the preexponential factor (*A*) and the Avrami exponent (*n*)) for the three stages were evaluated using model-free and model-fitting analysis. The insignificant variation of *n*, *E*, and *A* with extent of conversion during the progress of first peak crystallization shows that this stage of transformation can be described by single-step mechanism of crystallization. For the subsequent stages of crystallization, the behavior of the kinetic parameters indicates that multi-step mechanisms are involved in the transformation. Based on the model-fitting analysis of the present data, the reaction models, $g(\alpha)$, describing the crystallization stages is the Avrami-Erofeev model.

(Received July 17, 2015; Accepted September 14, 2015)

Keywords: Chalcogenide glass;Differential scanning calorimetry (DSC); Model-free kinetics; Model-fitting kinetics; Crystallization.

1. Introduction

Differential scanning calorimetry (DSC) technique is widely used to study thermal properties of glassy materials. This kinetic study can provide important information on nucleation and growth mechanisms associated with crystallization process in glasses. Such information is essential to gain proper understanding of the fundamental issues related to the nature of crystallization as well as to obtain glasses with better characteristics for a variety of technological applications [1,2].

The rising interest in the glassy Cu-As-Te systems can be attributed to the possible applications on thermoelectric devices [3,4] and other practical applications. The complexity of crystallization processes in these systems attracted the attention of many authors [3-20]. Multiple exothermic peaks are widely observed in the DSC experiments.

The objective of this paper was to study the kinetics of crystallization in $Cu_{18}As_{30}Te_{52}$ chalcogenide glass using model-fitting and model-free methods to provide clues about crystallization mechanism. DSC nonisothermal experiment will be analyzed to evaluate the kinetic parameters and the reaction model that can be used to describe the crystallization processes.

*Corresponding author: elabbar60@yahoo.com

2. Experimental

Bulk material was prepared by the well-established melt-quench technique. High purity (99.999%) Te, As and Cu in appropriate atomic percentage proportions were weighed and sealed in a quartz glass ampoule under a vacuum of 10^{-5} Torr. The contents were heated to about 1250 K for 36 h. During the melt process, the tube was frequently shaken to homogenize the resulting alloy.

DSC experiments were performed using Shimadzu DSC-60 instrument, with a temperature accuracy of ±0.1 K under dry nitrogen supplied at a rate of 35 mil/min. The samples, 2-3 mg, were encapsulated in standard aluminum pans. Nonisothermal DSC curves were obtained at selected heating rates between 3–99 K/min. The temperature and enthalpy calibrations were checked with indium (T_m = 429.75 K, ΔH_m = 28.55 J/g) as a standard material supplied by Shimadzu.

The structure of the samples was examined using a Shimadzu XRD-6000 X-ray diffractometer using Cuk_α radiation $\left(\lambda = 1.5418\, A^\circ\right)$. The X-ray tube voltage and current were 40 kV and 30 mA, respectively.

Qualitative and quantitative calculations were performed using the EDX technique accomplished with SEM from the displayed characteristic X-ray pattern. The results obtained are shown in Fig. 1. The composition of the alloy was determined and found to be 18, 30 and 52 at.% for Cu, As and Te, respectively.

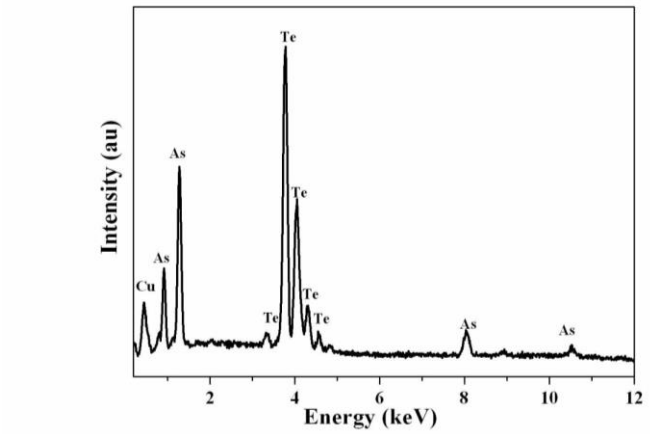

Fig. 1. EDX results of the chalcogenide $Cu_{18}As_{30}Te_{52}$ glass.

3. Results and discussion

DSC measurements were conducted on samples of $Cu_{18}As_{30}Te_{52}$ by heating from room temperature to about 700 K, at heating rates of 3 to 99 K/min. Fig. 2 shows typical DSC outputs obtained at different heating rates. Three exothermic peaks were observed. This complex behavior indicates that the transformation from the amorphous phase to the crystalline state is a multi-stage process. The three exothermic peaks shift to higher temperatures as the heating rate increases. This characteristic temperature shift can be used to extract the effective activation energies of the crystallization processes of the multi-step transformation from amorphous to crystalline phase using the widely used Kissinger method. More insight on the crystallization process can be obtained using different kinetic analysis involving model-fitting and model-free methodologies.

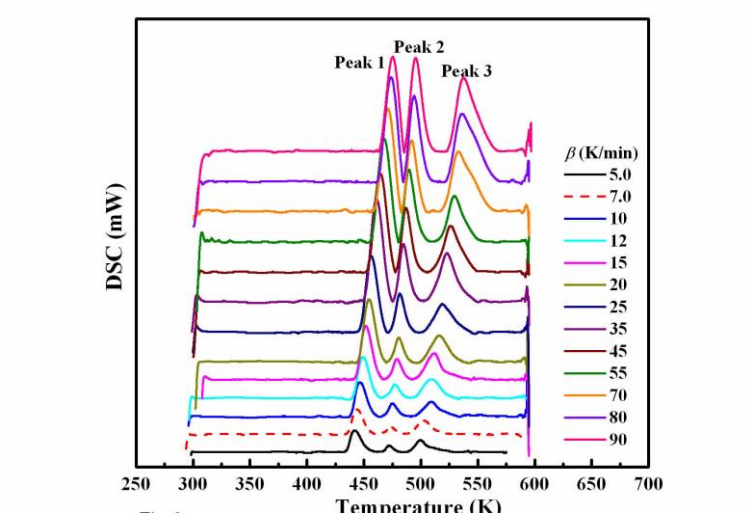

Fig. 2. DSC outputs for the chalcogenide $Cu_{18}As_{30}Te_{52}$ glass. Three crystallization peaks are observed at different heating rates.

3.1 Effective activation energy of crystallization

3.1.1 Kissinger's method

The crystallization kinetics of the three peaks can be analyzed using Kissinger equation. The effective activation energy of crystallization is obtained from the following relationship [21,22]:

$$\ln\left(\beta/T_p^2\right) = const. - \frac{E}{RT_p} \tag{1}$$

where T_p is the peak temperature and R is the gas constant. Therefore, a plot of $\ln(\beta/T_p^2)$ against $1/T_p$ should be a straight line and the effective activation energy can be calculated from the slope. Fig. 3 shows the Kissinger plots for the three peaks. The experimental data for the three peaks can be fitted to Eq.1 for the entire range of the heating rates. The effective activation energies as obtained from the fit are given in Table 1.

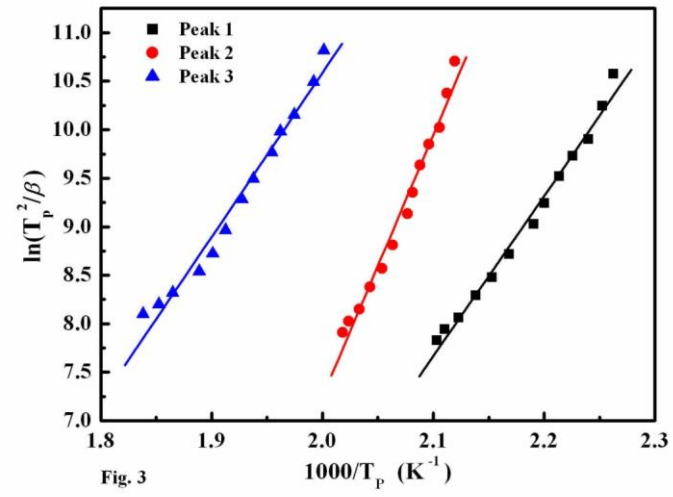

Fig. 3. Kissinger plots for the three stages of crystallization. The straight lines are fits to Eq.1.

Table 1 Crystallization activation energies, E, for the three stages of crystallization process.

Crystallization peak	*E* (kJ/mol.) Kissinger's eq.	*E* (kJ/mol.) Isoconversional
Peak 1	137	143
Peak 2	224	223
peak 3	140	141

3.1.2 Model-free method

The advanced isoconversional method introduced by Vyazovkin is a reliable model-free method widely used for the calculation of the effective activation energy of thermally activated reactions [23-24]. The effective activation energy can be determined at any particular value of α by finding the value of $E(\alpha)$ which minimizes the following objective function:

$$\Omega = \sum_{i=1}^{n} \sum_{j \neq i}^{n} \frac{I\left(E_\alpha, T_{\alpha i}\right)\beta_j}{I\left(E_\alpha, T_{\alpha j}\right)\beta_i}, \tag{2}$$

where *n* in Eq. 2 is the number of experiments carried out at different heating rates. These experiments are the extent of conversion as a function of temperature, $\alpha(T)$, represented in Fig. 4, for peak 1.

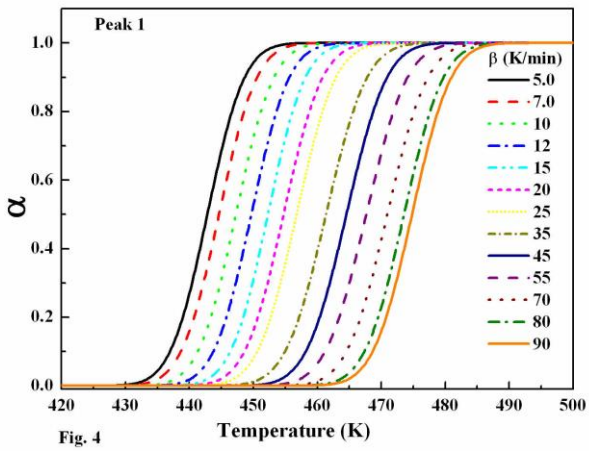

Fig. 4. α(T) dependence for the first crystallization peak (peak 1) at different heating rates.

The temperature integral, *I*, was evaluated using an approximation suggested by Gorbachev [25]:

$$I = \int_0^T \exp\left(\frac{-E}{RT}\right) dT = \frac{RT^2}{E + 2RT} \exp\left(\frac{-E}{RT}\right) \tag{3}$$

The variation of the effective activation energy with extent of conversion for the three peaks is shown in Fig. 5. No significant variation of $E(\alpha)$ with α is observed. The average values of the effective activation energies are presented in Table1 along with the values obtained using the Kissinger equation. It is evident that both methods (Kissinger and isoconversional) led to similar values of the effective activation energies for the three peaks.

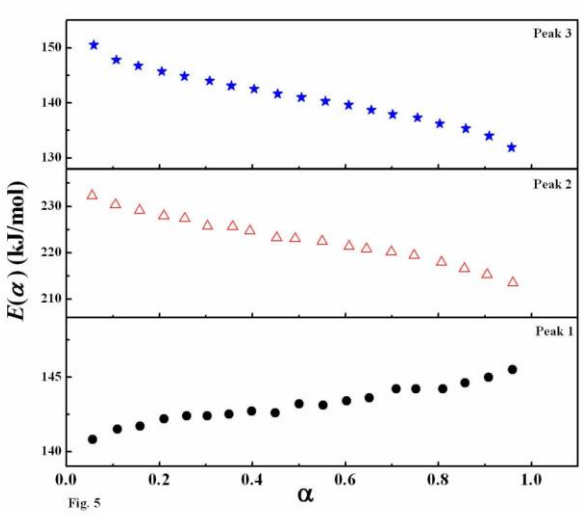

Fig. 5. Dependence of the effective activation energy for crystallization, E(α), on the extent of conversion, α, for peaks 1,2 and 3

3.2 The Avrami exponent (*n*)

The Avrami exponent *n* plays a key role in the analysis of overall crystallization kinetics. For example, the variation of *n* with heating rates and/or extents of conversion can provide further insight into the crystallization process.

According to a theory developed by Vazquez et al [26], the heating rate dependence of *n* can be obtained using the following equation:

$$n = RT_P^2 (d\alpha / dt)_P [(1-\alpha_P)^{(\delta_i+1)/\delta_i} \beta E]^{-1} \quad (4)$$

where the subscription *p* denotes the values of the quantities are those corresponding to the maximum crystallization rate. The impingement factor δ_i can be calculated from [26]:

$$1-\alpha_p = \left(\frac{\delta_i}{\delta_i+1}\right)^{\delta_i} \quad (5)$$

The impingement factor δ_i can be calculated using the iteration method of Eq. 5 using the experimental values of α_p. The values of δ_i for the three peaks are given in Table 2 for each heating rate. Therefore, the value of *n* can be found using the experimental values of the maximum transformation rate $(d\alpha/dt)_p$, degree of conversion α_p and the corresponding peak temperature T_p, at each heating rate along with the average value of the effective activation energy, *E*, and the impingement factor δ_i. The calculated values of *n* at different heating rates for the three stages of crystallization are given in Table 3.

Table 2 The heating rate dependence of the extent of conversion α_p corresponding to the maximum crystallization rate, the impingement factor δ_i and impingement exponent γ_i for the three stages of crystallization.

Crystallization Peak	Quantity β (K/min)	α_p	δi	γi
Peak 1	5.0	0.42348	0.50337	2.98661
	7.0	0.43750	0.56428	2.77217
	10	0.42832	0.52337	2.91068
	12	0.46476	0.71331	2.40192
	15	0.45217	0.63869	2.5657
	20	0.47999	0.82052	2.21873
	25	0.47714	0.79920	2.25185
	35	0.48505	0.86123	2.16112
	45	0.49858	0.95835	2.04346
	55	0.50129	1.01346	1.98672
	70	0.50451	1.04836	1.95387
	80	0.52148	1.26639	1.78964
	90	0.55113	1.86949	1.53490
Average	---	0.47867 ± 0.04	0.89077 ± 0.4	2.27518 ± 0.4
Peak 2	5.0	0.43550	0.55508	2.80154
	7.0	0.47526	0.78492	2.27401
	10	0.44761	0.61429	2.62790
	12	0.48473	0.85853	2.16478
	15	0.45007	0.62729	2.59415
	20	0.46145	0.69260	2.44382
	25	0.46409	0.70901	2.41043
	35	0.45309	0.64379	2.55329
	45	0.44902	0.62169	2.60852
	55	0.43651	0.55968	2.78673
	70	0.45828	0.67350	2.48478
	80	0.45752	0.66900	2.49477
	90	0.46508	0.71531	2.39800
Average	---	0.45678 ± 0.5	0.67113 ± 0.1	2.51098 ± 0.2

	5.0	0.42879	0.52537	2.90340
	7.0	0.45082	0.63123	2.58405
	10	0.49376	0.93834	2.06571
	12	0.51974	1.24089	1.80580
	15	0.54235	1.64906	1.60641
	20	0.49245	0.92614	2.07974
Peak 3	25	0.43017	0.53138	2.88190
	35	0.45979	0.68250	2.46520
	45	0.43602	0.55748	2.79378
	55	0.43177	0.53828	2.85777
	70	0.49538	0.95385	2.04838
	80	0.49494	0.94954	2.05314
	90	0.49775	0.97705	2.02349
Average	---	0.47490 ± 0.04	0.85393 ± 0.9	2.32067 ± 0.4

Table 3 The calculated values of n using Eq.4 at different heating rates for the three stages of crystallization.

β (K/min)	$n(\alpha)$ from Eq. (4)		
	Crystallization Peaks		
	Peak 1	Peak 2	Peak 3
5.0	2.91 ± 0.03	2.91 ± 0.07	2.81 ± 0.09
7.0	2.87 ± 0.02	2.46 ± 0.06	2.66 ± 0.09
10	2.91 ± 0.03	2.46 ± 0.06	2.36 ± 0.08
12	2.93 ± 0.03	2.37 ± 0.06	2.51 ± 0.09
15	3.00 ± 0.02	2.37 ± 0.06	2.47 ± 0.09
20	2.91 ± 0.03	2.55 ± 0.06	2.38 ± 0.08
25	2.92 ± 0.03	2.64 ± 0.06	2.24 ± 0.08
35	2.86 ± 0.02	2.44 ± 0.06	2.25 ± 0.08
45	2.93 ± 0.03	2.55 ± 0.06	2.47 ± 0.09
55	2.92 ± 0.03	2.34 ± 0.05	2.68 ± 0.09
70	3.01 ± 0.03	2.55 ± 0.06	2.01 ± 0.07
80	3.03 ± 0.03	2.30 ± 0.05	2.07 ± 0.07
90	3.06 ± 0.03	2.17 ± 0.05	2.20 ± 0.08
Average	2.94 ± 0.06	2.47 ± 0.2	2.39 ± 0.2

This shows that in each stage of crystallization the value of *n* does not change significantly with heating rate. This observation is also confirmed from the behavior of *n* at different extents of conversion of each peak. As shown by Lu et al [27], the variation of *n* with α can be found using the following expression:

$$n(\alpha) = \frac{-R\partial ln[-ln(1-\alpha)]}{E(\alpha)\partial(1/T)} \tag{6}$$

Figs. 6 a-c show such variation for the three peaks. It is evident from these figures that little variation of *n* with α is observed for peak 1. This indicates that while the stage of transformation represented by the first peak can be described by a single-step crystallization process, the second and third stages involve multistep crystallization process. An average value of *n* = 3, 2.5, and 2.4 can be assigned to the three processes of peaks 1,2, and 3, respectively. These values are similar to the corresponding values obtained from the heating rate dependence of *n* (Table 3).

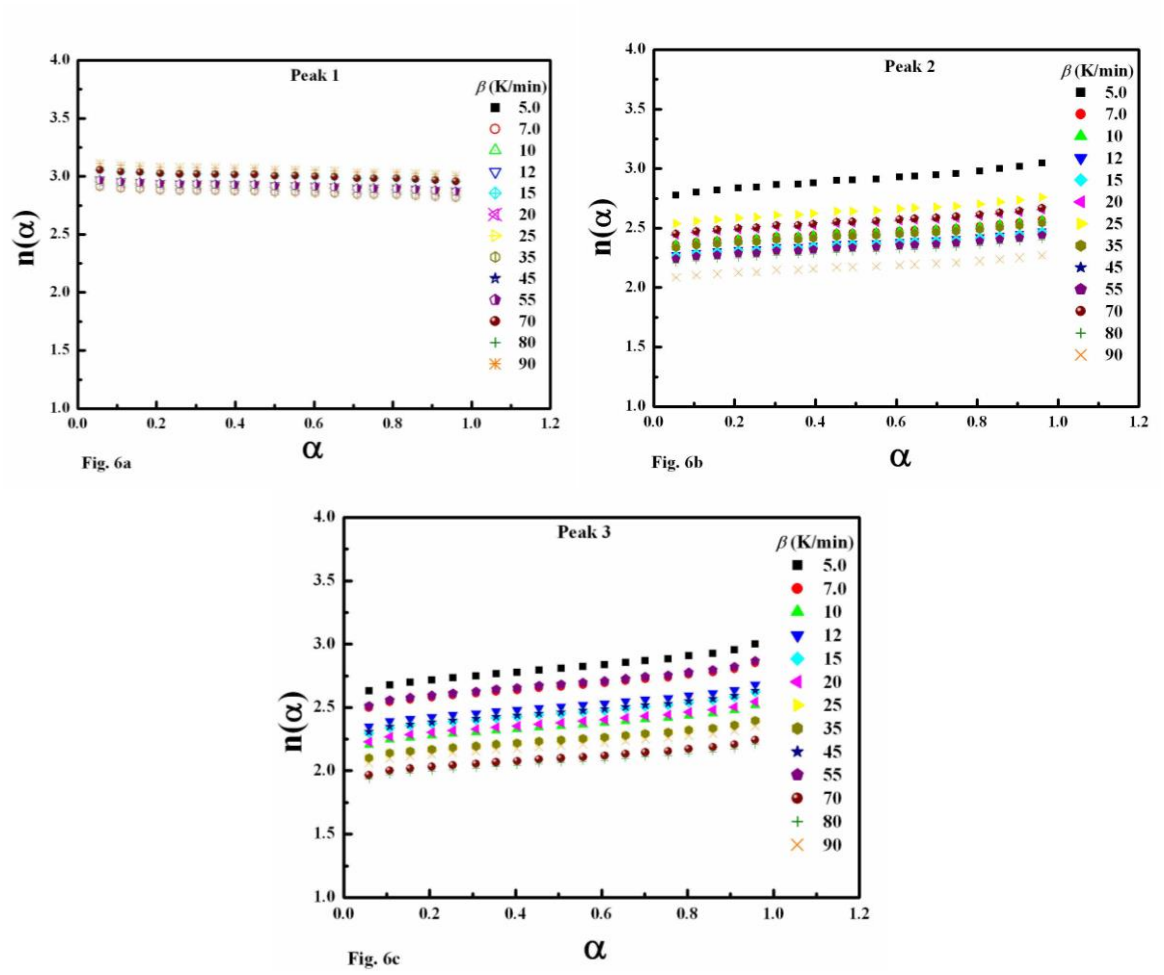

Fig. 6. The dependence of the Avrami exponent (n) on the degree of conversion (α) for the first (a), second (b) and third (c) crystallization peaks.

3.3 Model-fitting analysis

To describe the crystallization process more precisely, and to distinguish which one of the several kinetic models (listed in Table 4) can be used for the process, it will be useful to analyze the integral form of the reaction model, $g(\alpha)$, that is normally used to describe the kinetics of phase transformation in solids.

Table 4 Algebraic expressions of f(α) and g(α) for the reaction models considered in the present work.

No.	Symbol	Reaction model	$f(\alpha)$	$g(\alpha)$
Power law				
1	P1	n = 1/4	$4\alpha^{3/4}$	$\alpha^{1/4}$
2	P2	n = 1/3	$3\alpha^{2/3}$	$\alpha^{1/3}$
3	P3	n = 1/2	$2\alpha^{1/2}$	$\alpha^{1/2}$
4	P4	n = 3/2	$2/3\alpha^{-1/2}$	$\alpha^{3/2}$
Phase-boundary controlled reaction				
5	R1	Contracting linear	1	α
6	R2	Contracting area	$2(1-\alpha)^{1/2}$	$[1-(1-\alpha)^{1/2}]$
7	R3	Contracting volume	$3(1-\alpha)^{2/3}$	$[1-(1-\alpha)^{1/3}]$
Chemical reaction				
8	F1	First-order (Mampel)	$(1-\alpha)$	$-\ln(1-\alpha)$
9	F3/2	Three-halves order	$(1-\alpha)^{3/2}$	$2[(1-\alpha)^{-1/2}-1]$
10	F2	Second-order	$(1-\alpha)^{2}$	$[(1-\alpha)^{-1}-1]$
11	F3	Third-order	$(1-\alpha)^{3}$	$(1/2)[(1-\alpha)^{-2}-1]$
Avrami-Erofeev				
12	A3/2	$n = 1.5$	$(3/2)(1-\alpha)[-\ln(1-\alpha)]^{1/3}$	$[-\ln(1-\alpha)]^{2/3}$
13	A2	$n = 2$	$2(1-\alpha)[-\ln(1-\alpha)]^{1/2}$	$[-\ln(1-\alpha)]^{1/2}$
14	A3	$n = 3$	$3(1-\alpha)[-\ln(1-\alpha)]^{2/3}$	$[-\ln(1-\alpha)]^{1/3}$
15	A4	$n = 4$	$4(1-\alpha)[-\ln(1-\alpha)]^{3/4}$	$[-\ln(1-\alpha)]^{1/4}$
Diffusion				
16	D1	One-dimensional diffusion	$1/2\alpha$	α^{2}
17	D2	Two-dimensional diffusion	$1/[-\ln(1-\alpha)]$	$[(1-\alpha)\ln(1-\alpha)+\alpha]$
18	D3	Three-dimensional diffusion (Jander Eq.)	$3(1-\alpha)^{1/3}/2[(1-\alpha^{)-1/3}-1]$	$[1-(1-\alpha)^{1/3}]^{2}$
19	D4	Three-dimensional diffusion (Ginstling-Brounshtein)	$3/2[(1-\alpha)^{-1/3}-1]$	$(1-2\alpha/3)-(1-\alpha)^{2/3}$

The assumption that the transformation rate of a solid-state reaction in isothermal conditions is the product of two functions, one dependent on the temperature, *T*, and the other dependent on the conversion fraction, α, can be generally described by the following expression:

$$\frac{\mathrm{d}\alpha}{\mathrm{d}t} = k\left(T\right) f\left(\alpha\right), \tag{7}$$

where $k\left(T\right)$ is the reaction rate constant, $f\left(\alpha\right)$ is the reaction model, and α is the conversion fraction that represents the volume of the crystallized fraction. Under non-isothermal conditions with a constant heating rate of $\beta = \mathrm{d}T/\mathrm{d}t$, the kinetic equation combined with the Arrhenius approach to the temperature function of the reaction rate constant may be rewritten as:

$$\frac{\mathrm{d}\alpha}{\mathrm{d}T} = \frac{A}{\beta}\exp\left(-\frac{E}{RT}\right) f\left(\alpha\right), \tag{8}$$

where $A\left(\mathrm{s}^{-1}\right)$ is the preexponential (frequency) factor, $E\left(\mathrm{kJ\ mol}^{-1}\right)$ is the activation energy, and R is the universal gas constant. One can rearrange Eq. 8 and integrate by separation of variables, obtaining the $g\left(\alpha\right)$ as:

$$g(\alpha) = \int_0^{\alpha} \frac{d\alpha}{f(\alpha)} = \frac{A}{\beta} \int_{T_0}^{T} exp\left(-\frac{E}{RT}\right) dT$$
$$= \frac{AE}{R\beta} \int_0^x \frac{exp(-x)}{x^2} dx = \frac{AE}{R\beta} p(x) = \frac{A}{\beta} I(E,T) \quad (9)$$

The temperature integral $I(x)$ with $x = E/RT$ does not have an analytical solution. It can be determined using the Gorbachev approximation given in Eq. 3. One of the widely used model-fitting methods is the Coats-Redfern equation introduced by Coats and Redfern [28]. Utilizing the asymptotic series expansion for approximating the temperature integral $I(x)$. the following expression was suggested:

$$ln\frac{g(\alpha)}{T^2} = ln\left(\frac{AR}{\beta E}\left[1 - \frac{2RT^*}{E}\right]\right) - \frac{E}{RT} \quad (10)$$

where T^* is the mean experimental temperature. Eq. 10 is a generalization of the Coats-Redfern equation which was originally derived assuming the first-order reaction model $g(\alpha) = -\ln(1-\alpha)$. Plotting the left-hand side of Eq. 10 versus $1/T$ gives the activation energy E and the frequency factor A from the slope and intercept, respectively. The values of E and A simultaneously obtained using all reaction models presented in Table 4 are used to test the validity of the compensation effect for the present glass. The compensation effect (or isokinetic effect) which is widely reported in many glassy systems is represented by the following relationship between E and A [29]:

$$\ln A_m = a + bE_m \quad (11)$$

the subscript m refers to one of the possible reaction models $f(\alpha)$ assumed to described the process. Since the Arrehenius equation ($k = A\exp(-E/RT)$) can be expressed as:

$$\ln A = \ln k_{iso} + \frac{E}{RT_{iso}} \quad (12)$$

where k_{iso} is the isokinetic rate constant and T_{iso} is the isokinetic temperature. Therefore, the isokinetic parameters a and b of Eq. 11 are equivalents to $\ln k_{iso}$ and $1/RT_{iso}$. Fig 7 shows the plot of $\ln A_m$ versus E_m for all heating rates considered in this work.

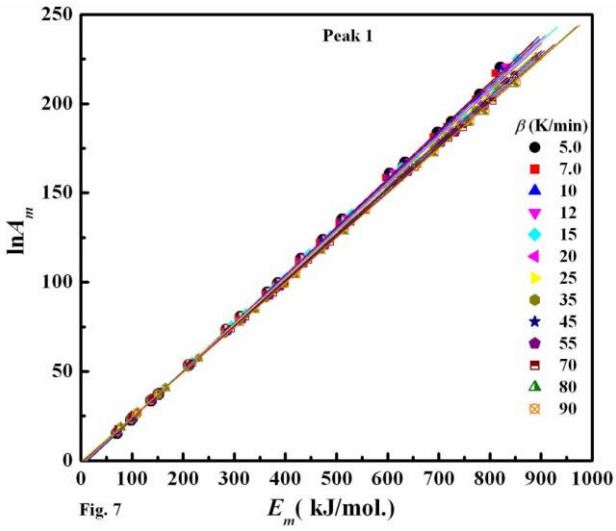

Fig. 7. The isokinetic relationship ($\ln A_m$ vs. E_m) for the first crystallization peak obtained at different heating rates

A linear relationship is observed confirming the validity of Eq. 11 for the present sample. Once the parameters *a* and *b* have been evaluated, the E_α values obtained from isoconversional analysis are substituted for E_m in Eq. 11 to estimate the corresponding $\ln A_\alpha$ values. Originally, this procedure was proposed by Vyazovkin and Lesnikovich [30] for estimating the pre-exponential factor in the isoconversional method. The pre-exponential factor, $A(\alpha)$ vs. α is shown in Fig. 8 for the three peaks. It is obvious in this

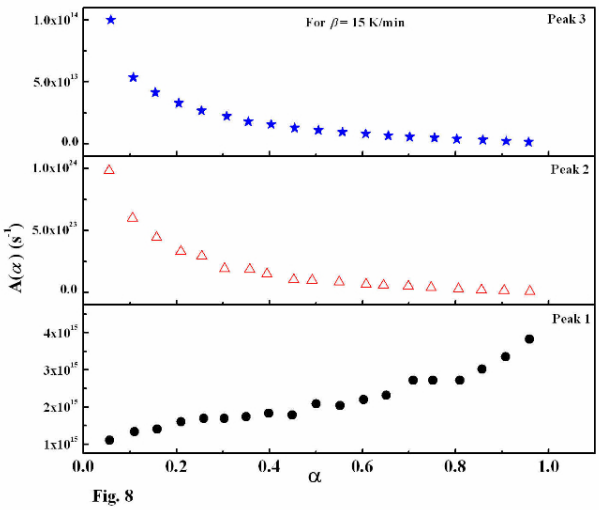

Fig. 8. The variation of the preexponential factor A(α) with extent of conversion α at heating rate of 15 K/min. for the three peaks

figure that the variation of $A(\alpha)$ as function of extent of conversion during the first peak (of the same order of magnitude ($x10^{15}$) for all values of α) is much smaller as compared with the $A(\alpha)$ variation during the crystallization stages of peak 2 and peak 3. This observation agrees very well with the results of section 3.2 as discussed above.

It is also possible to determine the appropriate reaction model which describes the crystallization stages represented by the observed three peaks using the masterplots method [28]. By using α = 0.5 as a reference point, and according to Eq. 9, we can write

$$g(0.5) = \frac{AE}{R\beta} p(x_{0.5}) \tag{13}$$

where $x_{0.5} = E/RT_{0.5}$ and $T_{0.5}$ the temperature corresponding to 50% conversion. Using Eqs. 9 and 13, the following equation is obtained

$$\frac{g(x)}{g(x_{0.5})} = \frac{p(x)}{p(x_{0.5})} \tag{14}$$

Therefore, plotting $\frac{g(x)}{g(x_{0.5})}$ versus α corresponds to theoretical masterplots of various $g(\alpha)$ functions. To draw the experimental masterplots of $\frac{p(x)}{p(x_{0.5})}$ versus α, the value of *E* and the temperature as a function of α of the process should be known in advance. Fig. 9a shows the $\frac{g(x)}{g(x_{0.5})}$ reconstructed from the experimental data (as symbols) and the corresponding reaction model chosen for peak 1. It is evident from Fig. 9a that the reaction model chosen for peak 1 is the Avrami–Erofeev (A3.0) model for the whole range of α. The excellent fit of the Avrami–Erofeev model with *n* = 3 to the experimental data of peak 1 is evident for all heating rates (5 – 90 K/min.) considered in this work. Similar analysis for the peaks 2 and 3 are shown in Figs 9b and 9c, respectively. In Fig. 9b, the experimental data follow very closely the theoretical masterplot corresponding to A3.0 reaction model for extent of conversion between 5 and 50% (α =0.05 to

0.5). For $\alpha \geq 0.5$, the crystallization process is described by A2.0 and A2.5 reaction models. According to Fig. 9c, peak 3 process can be described by A3.0 reaction model for $\alpha < 0.5$ and A2.0 reaction model for higher values α.

The values assigned to the Avrami exponent *n* obtained from the model-fitting analysis are very similar to the values obtained using model-free methods (see section 3.2 and Table 3). The above description of the kinetic behavior at different crystallization peaks can be further illustrated by evaluating the Avrami exponent (*n*) using the following equation [31],

$$\frac{1}{n} = \frac{\partial \ln[g(\alpha)]}{\partial \ln[-\ln(1-\alpha)]} \tag{15}$$

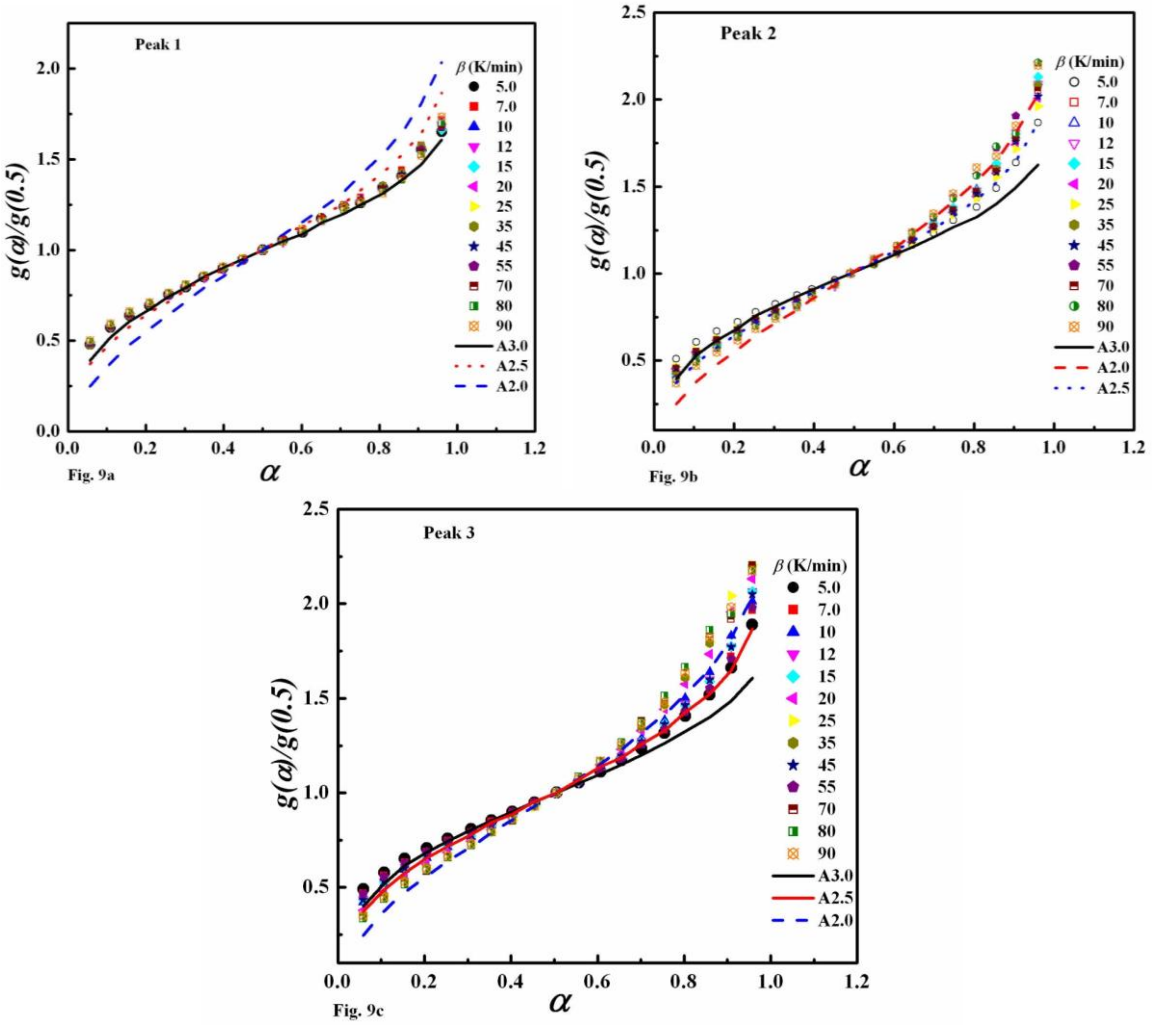

Fig. 9. g(α)/g(0.5) vs. α plots for the crystallization processes of peak 1 (a), peak 2 (b) and peak 3 (c) determined at different heating rates. (Solid lines are calculated using A3.0, A2.0, and A2.5 reaction models).

The dependence of the logarithmic form of the experimental reaction model ln[g(α)] on the theoretical ln[–ln(1-α)] for the three crystallization peaks is shown in Fig. 10. The values of *n* can be determined from the slopes of the straight lines obtained from the least squares fitting according to Eq. 15. The fact that the kinetics of the peak 2 and peak 3 process involve multi-step processes is clearly indicated by a cross-over in the kinetic behavior at $\alpha = 0.50$ with two different values of *n*. No such cross-over effect is observed for peak 1 process.

It is evident that crystallization in $Cu_{18}As_{30}Te_{52}$ system occurs in several steps as indicated by the multiple exothermic peaks in the DSC data (Fig.2). Similar observations were reported by

Wagner et al [12] in $Cu_{25}As_{30}Te_{45}$ and $Cu_{10}As_{45}Te_{45}$ glasses and Vazques et al [17] in $Cu_{20}As_{30}Te_{50}$ glass. The presence of two peaks in the exothermic thermal event was also reported by many authors [10, 15, 17, 20].

It had been suggested that [12,14] the structure of the glassy Cu-As-Te alloy can be described as a network of tetrahedral centered on copper atoms coexistence with other tetrahedral units whose centers are occupied by arsenic atoms. The tetrahedral units linked together by chains of tellurium atoms. Wagner et al [13] have proposed the following microstructural transformations corresponding to the three peaks: in the first stage of the process (peak 1), microcrystallites of As_2Te_3 are crystallized in an amorphous matrix. This is followed by a second stage (peak 2) in which Cu_7Te_5 is crystallized. Finally, in peak 3 stage, the volume fraction in the crystalline phase As_2Te_3 is increased. It is interesting to note the similar values of the effective activation energies for the crystallization stages (E) for the first and third stages of transformation. This is not surprising as the two stages involve nucleation and growth of As_2Te_3 phase.

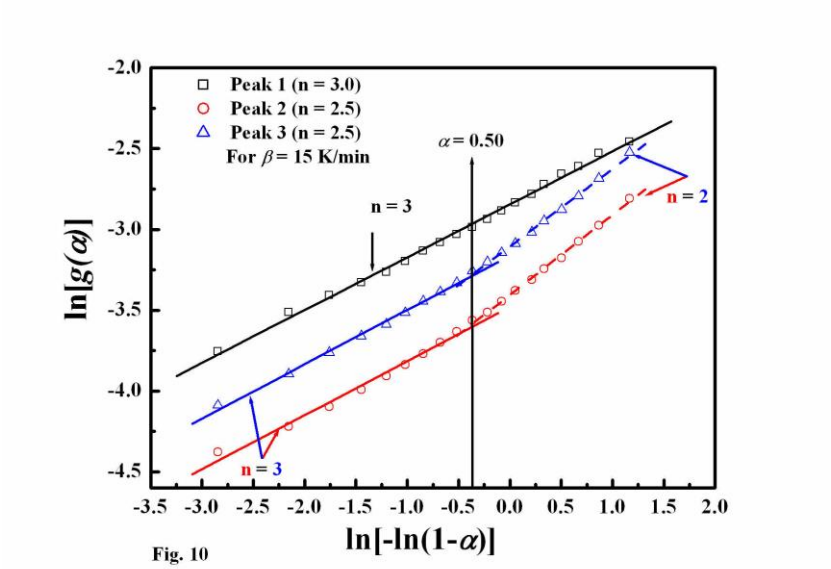

Fig. 10. ln[g(α)] vs. ln[-ln(1-α)] for the three crystallization peak. The experimental data (symbols) where determined at heating rate of 15 K/min. The values of n are determined from the least squares fitting using Eq. 15

4. Conclusions

The kinetics of crystallization of $Cu_{18}As_{30}Te_{52}$ were investigated using DSC technique. Three exothermic peaks in the DSC output were observed in this system, indicating the presence of three distinct stages of crystallization. The kinetic parameters for the three stages were evaluated using model-free and model-fitting analysis. The insignificant variation of n and E with extent of conversion during the progress of first peak crystallization shows that this stage of transformation can be described by single-step mechanism of crystallization. The behavior of the three kinetic parameters for the peak 2 and peak 3 stages of crystallization provided evidence that multi-step crystallization processes are involved during these stages of transformation. Based on the model-fitting analysis of the present data, the reaction models, g(α), describing the crystallization stages are A3.0 for peak1 for the entire range of α and A3.0 reaction model for $\alpha < 0.5$ and A2.0 reaction model for higher values α for peak 2 and peak 3 stages.

References

[1] P. Lucas, Z. Yang, M. K. Fah, T. Luo, S. Jiang, C. Boussard-Pledel, M. Anne, B. Bureau, Opt. Mater. Express **3**, 1049 (2013).
[2] S. Sen, T. G. Edwards, J. Y. Cho, Y. C. Joo, Te-Centric View of the Phase Change Phys. Rev. Lett. **108**, 1955061 (2012).
[3] J. B. Vaney, G. Delaizir, E. Alleno, O. Rouleau, A. Piarristeguy, J. Monnier, C. Godart, M. Ribes, R. Escalier, A. Pradel, A. P. Goncalves, E. B. Lopes, G. J. Cuello, P. Ziolkowski, E. Muller, C. Candolfi, A. Dauscher, B. Lenoir, J. Mater. Chem. **A1**, 8190 (2013).
[4] A.P. Goncalves , E.B.Lopes, G.Delaizir, J.B.Vaney, B.Lenoir, A.Piarristeguy, A. Pradel, J.Monnier, P.Ochin, C.Godart, J. Solid State Chem. **193**, 26 (2012).
[5] A. Giridhar, S. Mahadevan J. Non-Cryst. Solids **238**, 225 (1998).
[6] S. Mahadevan, A. Giridhar, J. Non-Cryst. Solids **221**, 281 (1997).
[7] M. P. Slankamenac, S. R. Lukic, M. B. Zivanov, Semicond. Sci. Technol. **24**, 085021 (2009).
[8] A. S. Soltan, A. H. Moharram, Physica B **349**, 92 (2004).
[9] M. V. Siljegovic, S. R. Lukic-Petrovic, G. R. Strbac, D. M. Petrovic, Phys. Scr. **T157**, 014027 (2013).
[10] L.A. Wahab, K. Sedeek, A. Adam, Mater. Chem. Phys. **59**, 232 (1999).
[11] C. Wagner, J. Vazquez, P. Villares, R. Jimenez-Caray, Mater. Lett. **16**, 243 (1993).
[12] C. Wagner, J. Vazquez, P. Villares, R. Jimenez-Caray, Mater. Lett. **18**, 280 (1994).
[13] C. Wagner, J. Vazquez, P. Villares, R. Jimenez-Caray, Phys. Scr. **54**, 118 (1996).
[14] J. Vazquez, P.L. Lopez-Alemany, P. Villares, R. Jimenez-Garay, Mater. Lett. **35**, 151 (1998).
[15] R. A. Ligero, J. Vazquez, P. Villares, R. Jimenez-Garay, J. Mater. Sci. **26**, 211 (1991).
[16] R. A. Ligero, J. Vazquez, P. Villares, R. Jimenez-Garay, J. Non-Cryst. Solids **124**, 63 (1990).
[17] J. Vazquez, R. A. Ligero, P. Villares, R. Jimenez-Garay, Thermochim. Acta, **157**, 181 (1990).
[18] N. Zotov, F. Bellido, M. Dominguez, R. Jimenez-Garay, A.C. Hannon, R. Sonntag, J. Phys. Chem. Solids **58**, 1625 (1997).
[19] N. Zotov, F. Bellido, M. Dominguez, A.C. Hannon, R. Sonntag, Physica B **276-278**, 463 (2000).
[20] A.A. Joraid , A.A. Abu-Sehly, M. Abu El-Oyoun, S.N. Alamri, Thermochim. Acta **470**, 98 (2008).
[21] H.E. Kissinger, J. Res. Nat. Bureau Standards **57**, 217 (1956).
[22] H.E. Kissinger, Anal. Chem. **29**, 1702 (1957).
[23] S. Vyazovkin, J. Comput. Chem. **22**, 178 (2001).
[24] S. Vyazovkin, J. Therm. Anal. Cal. **83**, 45 (2006) .
[25] V. M. Gorbachev, J. Therm. Anal. **8**, 349 (1975).
[26] J. Vazquez, D. Garcia-G.Barreda, P.L. Lopez-Alemany, P. Villares, R. Jimenez-Garay, Mater. Chem. Phys. **96**, 107 (2006).
[27] W. Lu, B. Yan, W. Huang, . Non-Cryst.Solids **351**, 3320 (2005).
[28] A.W. Coats, J.P. Redfern, Nature **201**, 68 (1964).
[29] R.K. AgrawalJ. Therm. Anal. Cal. **31**, 73 (1986).
[30] S.V. Vyazovkin, A.I. Lesnikovich, Thermochim. Acta **128**, 297 (1988).
[31] M. Abu El-Oyoun Mater. Chem. Phys. **131**, 495 (2011).